Applied Surface Science 507 (2020) 145032

Contents lists available at ScienceDirect

Applied Surface Science

journal homepage: www.elsevier.com/locate/apsusc

Full Length Article

Copper nanoparticles obtained by laser ablation in liquids as bactericidal agent for dental applications

M. Fernández-Arias[a,*], M. Boutinguiza[a,e], J. Del Val[a], C. Covarrubias[b], F. Bastias[b], L. Gómez[c], M. Maureira[b], F. Arias-González[d], A. Riveiro[a,e], J. Pou[a,e]

[a] Applied Physics Dpt., University of Vigo, EEI, Lagoas-Marcosende, Vigo E-36310, Spain
[b] Laboratory of Nanobiomaterials, Institute for Research in Dental Sciences, Faculty of Dentistry, University of Chile, Independencia, Santiago, Chile
[c] Laboratory of Microbiology, Department of Patology, Faculty of Dentistry, University of Chile, Independencia, Santiago, Chile
[d] School of Dentistry, Universitat Internacional de Catalunya, Barcelona, Spain
[e] Galicia Sur Health Research Institute (IIS Galicia Sur), SERGAS-UVIGO, Vigo, Spain

ARTICLE INFO

Keywords:
Copper nanoparticles
Noble metal nanoparticles
Laser ablation
Antibacterial effect

ABSTRACT

The dramatic increase of antibiotic-resistant bacteria is considered one of the greatest threats to human health at global scale. The antibacterial activity of noble metal nanoparticles, could be the solution against bacterial infectious diseases which currently do not respond to conventional treatments.

In this work, copper nanoparticles were produced by laser ablation using two different lasers. A nanosecond laser operating at 532 nm and a picosecond laser at 1064 nm were used to ablate a copper target submerged in water and methyl alcohol. The obtained colloidal solutions consisted of copper oxide nanoparticles in suspension with diameters ranging from few nanometers to 45 nm. The nanoparticles formation process is highly influenced by laser parameters, but the solvent plays a crucial role on their characteristics. Cu oxide nanoparticles obtained in water present chain-like nanostructure, while those obtained in methyl alcohol are spherical with lower presence of oxide. All the obtained nanoparticles are crystalline and noticeably stable.

Microbiology tests confirm their strong activity against *Aggregatibacter actinomycetemcomitans*. Cytocompatibility with human periodontal ligament stem cells is also confirmed. The biological assays evidence that ions release is not the main parameter responsible for the bactericidal activity of copper nanoparticles. Other factors such as oxidation state, size and crystallographic structure, have a greater influence on the process.

1. Introduction

Nowadays, more and more infections caused by resistant microorganism, fail to conventional treatments. According to the Centre for Disease Control and Prevention (CDC), antibiotic resistant bacteria cause at least 2 million infections per year with 23,000 deaths in the U.S. and 25,000 deaths in Europe [1]. The excess and improper use of antibiotics, has made the treatment of infections more difficult and expensive; some voices in the health system claim we are facing a new global health crisis [2,3]. In this sense, Gram-negative bacteria are a huge threat, because of the rapid evolution of their resistance mechanisms what results in insusceptibility to nearly all available antibiotics [4].

In dentistry, some of the more extended diseases caused by bacterial infections are periodontitis and periimplantitis. In both cases, the inflammation and destruction of soft and hard tissues surrounding teeth or dental implants, ultimately leads to loss of teeth or dental implant failure as the most common consequences [5]. Although many risk factors are related to the origin of periimplantitis [6], pathogenic microflora are the main cause of this periodontal disease [5]. *Aggregatibacter actinomycetemcomitans* is a Gram-negative bacteria and commonly part of the normal flora of human mouths, especially in gingival and supragingival crevices [7].

In light of this situation, it is necessary to explore new alternatives in the treatment of diseases caused by infections such as periimplantitis. Nobel metal nanoparticles have become an attractive alternative source to fight against such resistant microorganisms. The antibacterial activity of noble metal nanoparticles have been extensively studied because of their high surface to volume ratio, that increases reactivity allowing to kill the pathogens efficiently [8]. Particularly, copper nanoparticles are of special interest because they are potentially effective against different bacterial pathogens [8,9], and are very attractive in

* Corresponding author.
E-mail address: monfernandez@uvigo.es (M. Fernández-Arias).

https://doi.org/10.1016/j.apsusc.2019.145032
Received 29 July 2019; Received in revised form 7 December 2019; Accepted 10 December 2019
Available online 16 December 2019
0169-4332/

terms of cost when compared for example with Ag nanoparticles [10].

Although a great number of studies in the recent years have tried to explain the mechanisms of the bactericidal process, this still represents a gap in our knowledge. Previous researches have addressed that not only the size is behind this remarkable antibacterial activity, also shape and crystallographic structure of the nanoparticles [11], which depend on the fabrication method. In this sense, Laser ablation of solids in liquids (LASL) is a key technique to obtain pure nanoparticles with no need of chemical precursors which can contaminate the obtained material, resulting in a potential harmful agent not only for the target bacteria but also for the healthy tissues.

In previous works, other noble metal nanoparticles such as Ag NPs were obtained by means of laser ablation in open air [12] and water [13,14] and their bactericidal effects were demonstrated. Copper and copper oxide nanoparticles were already synthesized by laser ablation in different solvents such as distilled de-ionized water [15], acetone [16] or organic solutions such as phenanthroline [17]. These works show that the characteristic features of the obtained nanoparticles can be controlled by varying the laser parameters and the liquid properties. Although all of them demonstrate the bactericidal properties of copper nanoparticles, none of them establishes the relationship between bactericidal activity and physicochemical properties, neither their biocompatibility.

In the present work, the bactericidal properties of the Cu nanoparticles are evaluated against *A. actinomycetemcomitans* (a Gram negative bacteria) one of the main pathogens responsible for inducing localized aggressive periodontitis [18], peri-implantitis [5] and various non-oral infections [7]. In order to assess their biocompatibility, the cytotoxic effects were evaluated using human periodontal ligament stem cells. The mechanism responsible for the bacterial growth inhibition is also studied and discussed. The present study provides some insights as to the influence of nanoparticle size, morphology, oxidation state, crystallographic structure, stability and ion release on the biocidal process.

2. Materials and methods

2.1. Laser ablation

Copper foils with 99.99% of purity (Thermo Fisher Scientific), were used as laser ablation targets. In order to analyze the influence of the laser parameters and the liquid medium used in the process, the targets were submerged in two different solvents and ablated by two different diode-pumped Nd:YVO_4 laser sources.

Sample nomenclature with the corresponding assay conditions are listed in Table 1.

The first laser source was a nanosecond laser providing pulses at wavelength of 532 nm (Green – Nanosecond), with 0.26 mJ of pulse energy and 14 ns of pulse duration. The second laser source was a picosecond laser emitting radiation at 1064 nm (IR – Picosecond), with 0.03 mJ of pulse energy and 800 ps of pulse duration. The laser beam spot diameter on the target surface was estimated to be 132 μm giving a fluence of 1.90 J/cm^2 in case of Green – Nanosecond laser and 196 μm giving a fluence of 0.09 J/cm^2 for IR – Picosecond laser.

Processing parameters used with both lasers are listed in Table 2.

In the laser ablation process, pure deionized water and methyl alcohol were used as solvents. In order to assure the minimum energy loss as well as the complete cavitation bubble formation inside the solvent, the liquid layer thickness over the target was 2 mm in both cases. The experimental setup is shown in Fig. 1.

NPs were produced at room temperature and atmospheric pressure by using a rectangular scanning pattern of about 2.5 × 6 mm^2 with 90% overlapping. The ablated mass was determined by weighing the targets before and after the ablation process ($\Delta m \pm 0.001$ g). In all experiments, the laser beam was focused on the upper surface of the target and was kept in relative movement with respect to the metallic plate at 50 mm/s of scanning speed.

Table 1
Samples produced and analyzed.

Sample	Laser source	Solvent
a	Green – Nanosecond	Water
b	Green – Nanosecond	Methyl alcohol
c	IR – Picosecond	Water
d	IR – Picosecond	Methyl alcohol

2.2. Physicochemical characterization

2.2.1. Obtained nanoparticles

After each experimental assay, drops of the obtained solutions were deposited and allowed to dry on carbon-coated copper micro-grids and on Si substrates for examination of particle morphology and microstructure. Transmission electron microscopy (TEM), selected area electron diffraction (SAED) and high-resolution transmission electron microscopy (HRTEM) images were acquired with a JEOL JEM 2010F high-resolution transmission electron microscope equipped with a slow digital camera scan, using 200 kV accelerating voltage. Identification of phases was achieved by comparing the measured distances from SAED with the diffraction patterns from ICDD (JCPDS) database. Additionally, Field Emission Scanning Electron Microscopy (FESEM) images were taken with a JEOL JSM 6700F microscope. Nanoparticle size distribution derived from a histogram was obtained by measuring the diameter of about 400 particles from TEM images.

The UV-VIS absorption spectrum of the copper nanoparticles (Cu-NPs) in colloidal suspension was measured in the range from 190 to 800 nm in a Hewlett Packard HP 8452 spectrophotometer with 3.5 ml volume and 10 mm pathlength, by using a quartz cuvette previously washed.

The stability of each sample was studied by means of Z-Potential measurements obtained with a Zetasizer Nano ZS ZEN3600 (Malvern Instruments). The cuvette used in the measuring process was a DTS1060 capillary cell. Before each ZP measurement, the cell was cleaned with deionized water. Thereafter, the cell was filled with each sample completely and slowly, to avoid the formation of air bubbles. After measuring, the quantity of sample employed was rejected in order to prevent the sample degradation caused by the electrophoresis.

2.2.2. Immobilized nanoparticles

To conduct the biological assays, the obtained Cu-NPs (according to Table 1) were immobilized on plates of commercial pure titanium grade 4, (10 × 10 × 1 mm^3). To this purpose, the titanium plates were submerged in the colloidal solutions, covering the whole surface and allowing to evaporate at room temperature.

Coating and morphology of the particles on the Ti plates, were

Table 2
Laser parameters.

Laser source	Wavelength (nm)	Pulse length (ns)	Pulse frequency (kHz)	Pulse energy (mJ)	Scanning speed (mm/s)
Green – nanosecond	532	14	20	0.26	50
IR – picosecond	1064	0.8	200	0.03	50

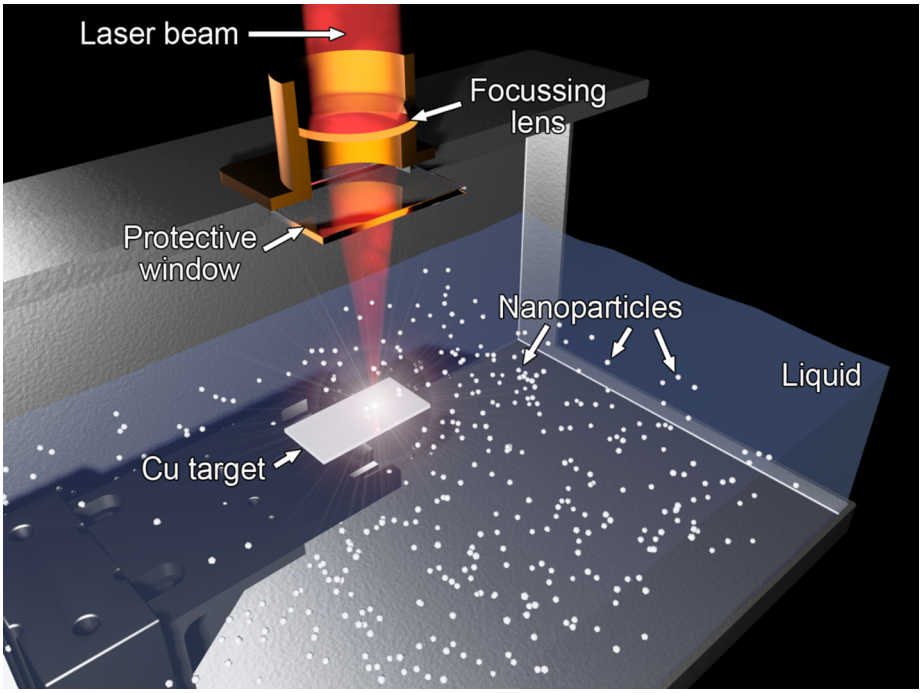

Fig. 1. Laser ablation experimental set-up.

characterized by using a Ga ion beam in an FEI Helios NanoLab 600 dual beam microscope. SEM images and energy dispersive spectroscopy of x-rays (EDS) about the sectioning layer of nanoparticles were obtained after protecting them from FIB (Focused Ion Beam) damage with an electron beam deposited Pt layer.

To study the influence of copper ions in the bactericidal process, copper ions release from the immobilized nanoparticles, was tracked. Since both media used in the bio response assays are different, distilled de-ionized water was used for that purpose. The titanium plates with each type of immobilized nanoparticles (3 pieces for each condition) were submerged in 25 ml of distilled de-ionized water.

In order to verify that the deposited nanoparticles are not detached from the surface during the assays, UV-VIS spectroscopy was also used. Absorbance of liquid in which the Ti plates were submerged, was measured regularly during the first 21 days with the purpose of detecting supernatants.

Afterwards, 3 ml of each sample were laid away regularly during 21 days. To ensure the non-presence of nanoparticles when quantifying the ion release, in addition to the spectrometry, this volume was also centrifuged by using an Eppendorf miniSpin centrifuge at 13,400 rpm for 30 min at room temperature. After centrifuging, only 2 ml from the upper surface of each sample were taken to analyze the ions content by inductively coupled plasma optical emission spectrometry (ICP-OES) with an Optima 4300 DV (Perkin Elmer). After sampling, removed volume was refilled with fresh water in order to keep a constant volume.

2.3. Bio response of the immobilized nanoparticles

The biological assays were conducted with the immobilized nanoparticles on titanium plates. Three replicas per condition were used to conduct each test.

The antibacterial properties of the obtained Cu-NPs were evaluated with a Gram negative bacterial strain *Aggregatibacter actinomycetemcomitans,* a representative pathogen of periimplantitis.

The strain was grown in BHI broth or agar (Brain Heart Infusion) and incubated in a 5% CO_2 atmosphere at 37 °C for 48 h. From a grown plate, bacteria were transferred to fresh BHI medium to a density equivalent to McFarland 0.5 standard. Each sterilized titanium sample was placed into glass tube with screw cap. Then, 3 ml of the inoculum were added to each tube, and incubated for 48 h in a 5% CO_2 atmosphere at 37 °C. After the incubation period, antibacterial activity was evaluated by total viable counts on each titanium surface. The titanium samples were removed from the tubes, washed 3 times with Phosphate Buffer Saline (PBS) and incubated with a 0.88 wt% NaCl solution and 1% Tween 80 for 10 min to detach the adherent bacteria from the titanium surfaces. Samples of 100 μL were taken from the bacterial suspension, diluted and plated in BHI agar. After 48 h of incubation at 37 °C in a 5% CO_2 atmosphere, the colonies were counted and the colony forming units per mL (CFUs) were calculated for each titanium surface.

Cytotoxic effects of the Cu nanoparticles were evaluated using human periodontal ligament stem cells (PDLSCs) within the same concentration used in the evaluation of the antibacterial properties. PDLSCs were isolated from surgically extracted human third molars extracted for orthodontic reasons at the Dental Clinical of the University of Chile following the procedure described elsewhere [19]. The cytocompatibility of the titanium surfaces in human dental pulp stem cells (hDPSC) was evaluated by reducing the salts of [3-(4,5-dimethyl-thiazol-2-yl)-5-(3-carboxymethoxyphenyl)-2-(4-sulfophenyl)-2H-tetrazolium] (MTS) and an electron coupling reagent (phenazine ethosulfate; PES) (CellTiter Aqueous One Solution cell proliferation assay kit from Promega). These assays were performed at 1 and 5 days of incubation of 2×10^4 cells with the titanium samples in Dulbecco's Modified Eagle Medium (DMEM) in a humidified 5% CO_2 atmosphere.

2.4. Statistical analysis

Data collected from the antibacterial assay and the cytocompatibility analysis were statistically analyzed. All quantitative values were presented as mean ± standard deviation (SD). All experiments were performed using three replicates. First, antibacterial activity was analyzed by Dunnett's test to compare the mean of each group with the mean of the control group with a level of significance p-value < 0.05. Afterwards, Tukey's test was applied to compare the means of all groups in pairs. In this case, two levels of significance p–value < 0.05 and p-

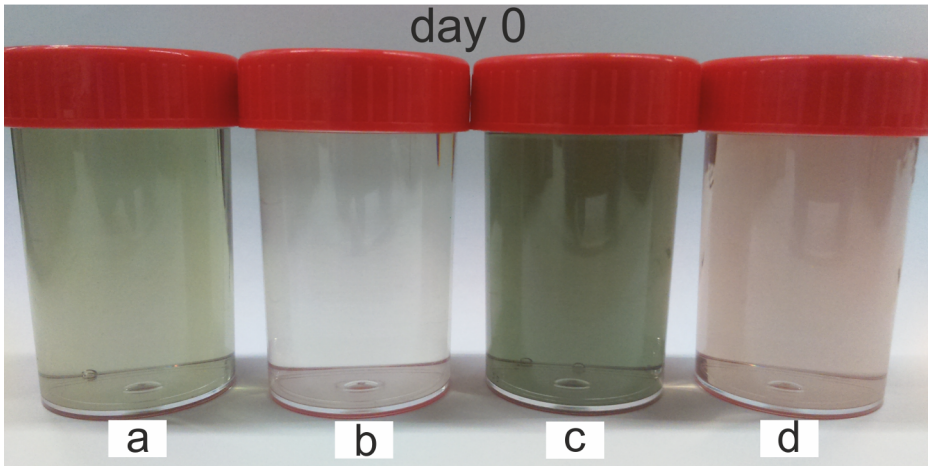

Fig. 2. Photograph of the Cu-NPs suspensions obtained by laser ablation using (a) Green – nanosecond laser in water, (b) Green – nanosecond laser in methyl alcohol, (c) IR – picosecond laser in water, (d) IR – picosecond laser in methyl alcohol. Images taken the day of production (day 0).

value < 0.01 were established. The viability of cells cultured on the samples was studied by means of one-way analysis of variance (ANOVA). The difference between group means were accepted as statistically significant when p-value < 0.05.

3. Results and discussion

Cu-NPs in suspension were produced by laser ablation in two different solvents without using any chemical precursors. Nanoparticle formation was directly detected because of the change in the solvent color, from colorless to the final coloring (see Fig. 2). The colloidal solutions obtained in water (a and c) exhibit greenish color indicating oxidized Cu. The nanoparticles obtained in methanol show lighter color due different level of oxidation and particle size.

Despite the different color of the obtained colloidal solutions, all of them present the same concentration. Since the process parameters (shown in Table 2) were adjusted to achieve the same concentration of nanoparticles (30 mg/L) for each sample, this can lead to particles with different properties.

3.1. Physicochemical characterization of the obtained nanoparticles by laser ablation

3.1.1. Morphology and size distribution

Several FESEM and TEM images were recorded and used to perform an analysis of morphology and size distribution. Representative FESEM and TEM micrographs of each obtained sample can be observed in Figs. 3 and 4 respectively.

Close inspection of Figs. 3 and 4 reveals that size and morphology of the particles obtained are deeply influenced by the laser parameters and the solvent.

In order to provide a deeper analysis, the diameters of more than 400 nanoparticles were measured from several TEM images of each sample and the resulting size distributions are shown in Fig. 5.

Cu-NPs obtained in methyl alcohol show small size and rounded shape. When water is used as solvent, the obtained nanoparticles exhibit a chain-like structure with larger mean size than the corresponding ones obtained in the same conditions but using methyl alcohol as solvent.

According to the effect of laser parameters on the resultant nanoparticles, it is noteworthy to mention that size decreases in both cases (water and methyl alcohol) if Green – Nanosecond laser is used, comparing with the case of using the IR – Picosecond laser.

This difference in size and shape reveals the mechanisms involved in the nanoparticle formation process. When the laser beam strikes on the copper plate, the incident radiation is absorbed, heating up the copper above its melting point. This heating leads to the plasma plume formation which is entirely confined within the liquid layer. In this process, the material on the surface of the plate is pulled out and confined by the surrounding liquid to nucleate and grow by coalescence [20]. Nucleation and growth of particles are governed by the cooling rate and the reaction between the species from the surrounding medium and the target. In this sense, although water possess at room temperature a higher heat transfer coefficient than methyl alcohol [21], results evidence the remarkable effects of the solvent molecules from the decomposition at high temperatures in the ablation process. While in water, molecular oxygen reacts with the ejected species from the target, leading to oxidation and allowing the coalescence; in methyl alcohol, carbon species (C*) take part covering the surface of the embryonic particles and stopping the growth of nuclei [20,22].

On one hand, the nanoparticle formation process is influenced by laser pulses duration. When nanosecond laser pulses impact on the material, there is a temporal overlap between the pulses and the ablation event. Therefore, in presence of a long laser pulse, the plasma plume can absorb part of the incoming laser energy, increasing the plasma temperature and boosting the atomization of the material, as reported in previous works, which evidences that the ablation process starts a few tens of picoseconds after the laser irradiation and the plasma lasts for tens of nanoseconds [23]. This process gives as a result NPs with small average diameters.

On the other hand, the absorption coefficient of copper is higher for a 532 nm radiation (green) than for a radiation of 1064 nm of wavelength (IR) [24]. The aforementioned effect could be potentially increased by the self-absorption process that takes place at 532 nm. Since Cu-NPs absorb part of the laser energy at 532 nm of wavelength, the final intensity reaching the surface of the target is reduced [25]. This process, although reduces the efficiency of laser ablation, resulting in fragmentation and consequently in smaller nanoparticles. On the contrary, the high overlapping of IR laser favors the appearance of the nanoparticle surface charge and determines the interaction between the plume species (ions, clusters, free atoms…) and nanoparticles during the ablation process. The growth process will be determined by the attractive and repulsive forces between them, being responsible for a broader size dispersion [16].

3.1.2. Crystallography and composition

All the particles obtained in the present work are crystalline. This aspect can be observed in the corresponding HRTEM micrographs (Fig. 6). As shown, when using water as a solvent in the laser ablation process (samples a and c), the clear crystalline interface continuity

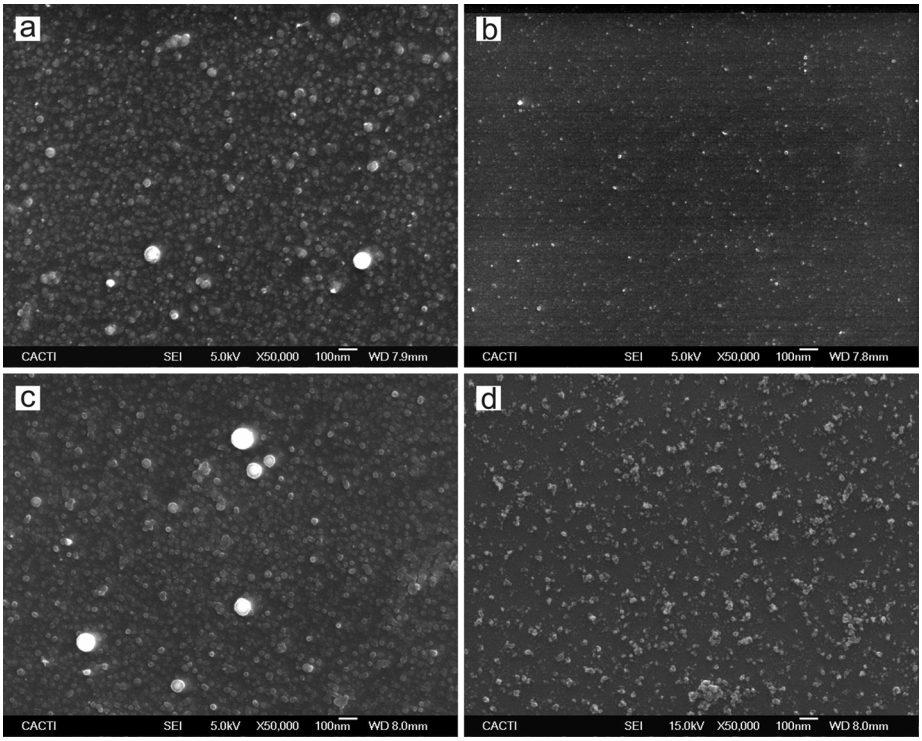

Fig. 3. FESEM micrographs of Cu nanoparticles obtained by laser ablation using (a) Green – nanosecond laser in water, (b) Green – nanosecond laser in methyl alcohol, (c) IR – picosecond laser in water, (d) IR – picosecond laser in methyl alcohol.

between particles corroborates the slow cooling during the particles growth process. On the contrary, samples (b and d) obtained in methanol seem to be a combination of different crystallographic orientations.

Regarding the nanoparticle composition, the measured interplanar distances and the corresponding FFT of single particles, confirmed that the predominant lattice spacing can be indexed to cubic Cu_2O in case of using water as solvent and metallic copper in case of methanol. In addition, the presence of a carbon layer around the nanoparticles when methanol is used as solvent is signaled with red arrows.

In order to elucidate the crystalline phases of each sample, SAED was performed on several groups of particles as shown in Fig. 7. The measured interplanar distances from Fig. 7 are listed in Table 3. According to the data collected in Table 3, the main reflections of each sample correspond with diffraction patterns of metallic copper and different oxidation states of copper from ICDD (JCPDS) database.

Note that, main reflection *hkl* of Cu-NPs obtained by laser ablation using Green – nanosecond laser in water (sample a), can be indexed on the cubic crystal lattice of Cu_2O (JCPDS-ICDD ref. 005-0667), corresponding to a combination of cubic Cu_2O and monoclinic CuO (JCPDS-

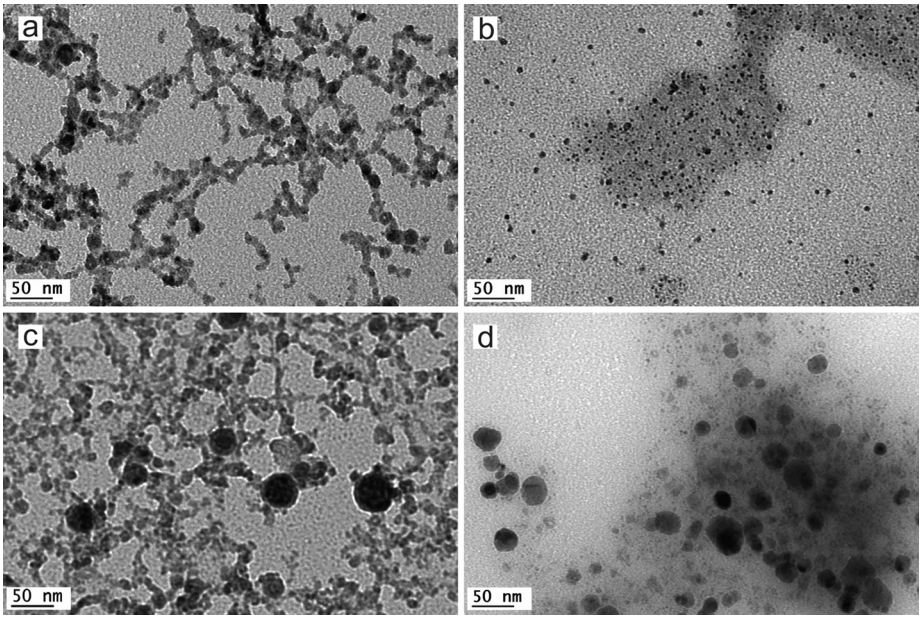

Fig. 4. TEM micrographs of Cu nanoparticles obtained by laser ablation using (a) Green – nanosecond laser in water, (b) Green – nanosecond laser in methyl alcohol, (c) IR – picosecond laser in water, (d) IR – picosecond laser in methyl alcohol.

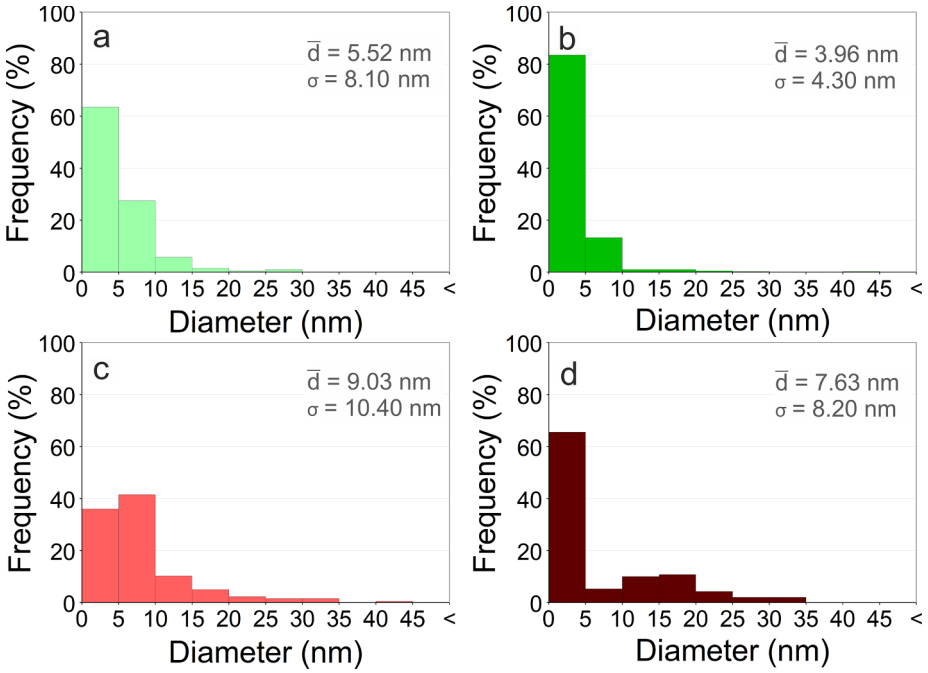

Fig. 5. Size distribution of Cu nanoparticles obtained by laser ablation using (a) Green – nanosecond laser in water, (b) Green – nanosecond laser in methyl alcohol, (c) IR – picosecond laser in water, (d) IR – picosecond laser in methyl alcohol.

ICDD ref. 041-0254) if IR – picosecond laser is used (sample c).

Otherwise, the indexation of the main reflections of Cu-NPs obtained by laser ablation using the IR – picosecond laser in methyl alcohol (sample d), corresponds to metallic copper with cubic unit cell (JCPDS-ICDD ref. 004-0836) and presence of copper oxide.

Despite the fact that copper oxidation also takes place when Green – nanosecond laser is used in methyl alcohol (sample b), it is clearly evident that Cu-NPs present higher oxidation state when water is used as solvent than when methyl alcohol is utilized. These results corroborate that the use of alcohol as solvent in the LASL prevent the total oxidation of the NPs.

These results are in good agreement with previous ones obtained by Marzun et al. which evidence that the nanoparticle oxidation during laser synthesis, is mainly caused by reactive oxygen species from the decomposition of the liquid medium as a result of the laser interaction with the solvent [22]. In this sense, while water molecules decompose into reactive oxygen species, methanol molecules can release carbon atoms in the plasma. These carbon atoms form a layer around Cu nanoparticles and act as an oxygen scavenger.

3.1.3. Optical properties

In general, metal nanoparticles have unique features under electromagnetic radiation [26]. In order to study the optical properties of the obtained nanoparticles, the absorption of each sample was measured in the range of 190–800 nm by UV-visible spectroscopy. The UV-VIS absorbance spectra of the obtained solutions are shown in Fig. 8.

Due to the surface plasmon resonance (SPR) effect, the Cu-NPs absorption is normally within the range of 500–600 nm, while Cu_2O NPs show absorption in the range of 300–500 nm [27] and CuO NPs between 250 and 300 nm [28–30]. However, the exact position of the absorption peak depends on stability and particle size, being around 560 nm if Cu-NPs diameter is ranging between 10 and 40 nm [31].

Note that samples obtained in methyl alcohol (samples b and d), present similar absorbance profiles. The first absorbance peak, observed at 250 nm can be ascribed to CuO NPs while the second peak at 380 nm clearly corresponds to Cu_2O NPs [28]. Despite the indexation of the Cu-NPs obtained in methyl alcohol with the IR – picosecond (sample d) substantially corresponds to metallic copper, the spectrum shows no peak at 560 nm.

Regarding the Cu-NPs obtained by using the Green – nanosecond laser in water (sample a), a maximum absorption peak appears at 230 nm of wavelength. It is worthwhile to mention that most works previously reported [21–24], show only values from 290 nm to 800 nm without taking into account the UV region between 190 and 290 nm. In this sense, when absorbance measurements of Cu_2O NPs are made in this range, a peak near to 210 nm appears [32].

Additionally, Cu-NPs obtained by laser ablation with the IR – picosecond laser in water (sample c), exhibit two absorption peaks. While the first peak at 200 nm seems to correspond with Cu_2O NPs, the second one at 300 nm matches with the characteristic absorbance peak of CuO NPs.

In order to study the stability of the colloids, suspensions were stored in darkness without stirring during 14 days. Fig. 9.A shows how the colloidal suspensions look like after the storage time. Note that the appearance of the samples has changed from day 0 (see Fig. 2). Whereas Cu-NPs obtained by laser ablation with Green – nanosecond laser in water are precipitated (sample a), those obtained in water by using IR – picosecond laser (sample c) have changed the color from dark green to yellowish brown (Fig. 9B), which at first sight seems to suggest a higher state of oxidation. Furthermore, colloidal Cu-NPs obtained in methyl alcohol (samples b and d) seem to form small aggregates staying in suspension without relevant change in color. These aggregates disintegrate instantly when submerged in ultrasonic bath at room temperature, as evident from the Fig. 9B.

According to the preliminary inspection, spectrophotometric analysis of sonicated colloidal suspensions after 14 days shows in rough outlines, no change in the absorbance (see Fig. 10). Only the suspension obtained by laser ablation with Green – nanosecond laser in water (sample a) shows a change of its absorbance spectrum. On one hand, the absorbance peak is notably softened which is indicative of degradation because of a change in the oxidation state [22,33]. On the other hand, the broad absorption peak is red shifted. This shifting nearby 500 nm of wavelength may be attributed to agglomeration, which contributes to increase the particle size [33]. As copper is highly sensitive to oxidation, the obtained nanoparticles in aqueous medium undergo first stage oxidation in their nucleation. With aging, oxidation

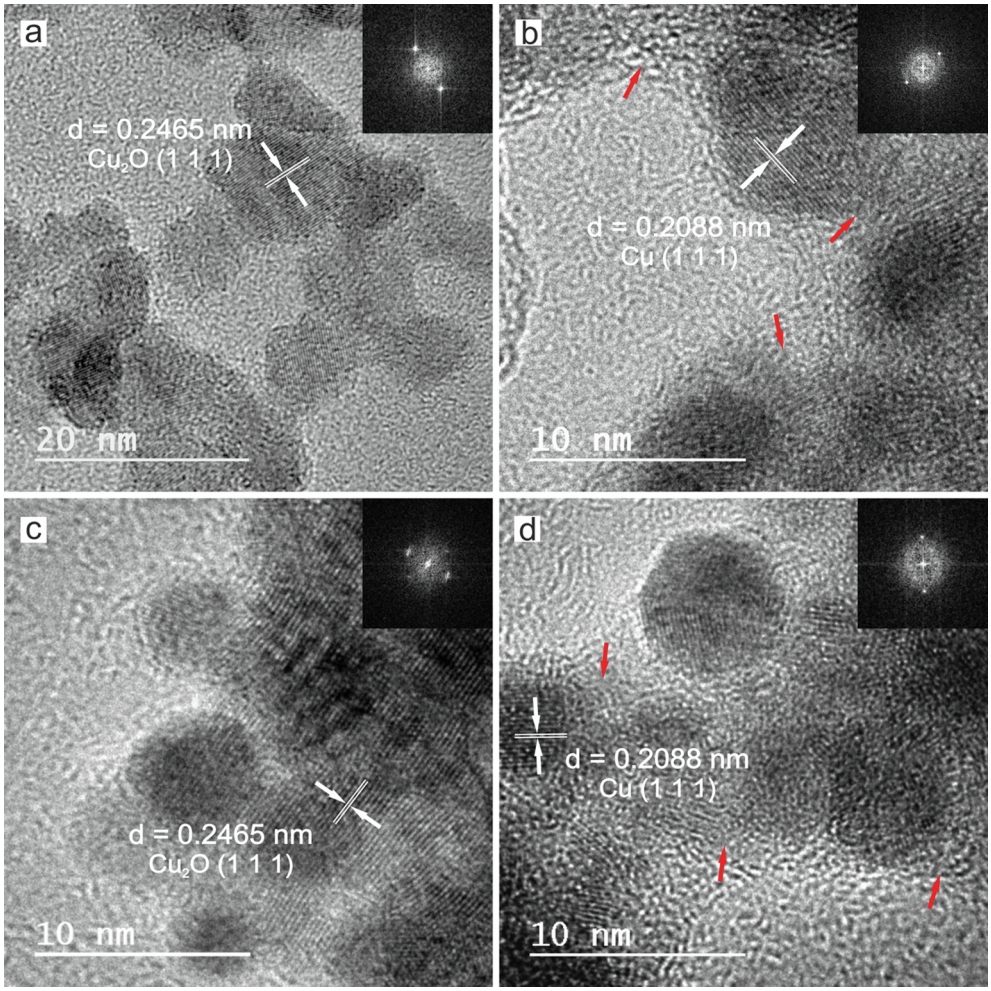

Fig. 6. HRTEM of Cu nanoparticles obtained by laser ablation. Processing conditions correspond to those collected in Table 1. Measured interplanar distances and the corresponding FFT of single nanoparticles (inset). Red arrows indicate the presence of amorphous carbon. (For interpretation of the references to colour in this figure legend, the reader is referred to the web version of this article.)

continues to transform the initial nanoparticles obtained in water into CuO ones. In this sense, the lack of changes in the UV-vis absorbance despite the appearance modification of the suspension obtained in water with IR – picosecond laser, can be attributed to a change in the Cu_2O and CuO proportion [34].

On its behalf, the nanoparticles obtained in methanol showed more disparity and smaller size than those obtained in water under the same conditions. As it was previously mentioned, the highly exited species (C*) ablated from methanol can act as capping layer limiting the growth of nanoparticles and preventing them from total oxidation. This is also consistent with their stability and formation of kind of non-precipitated chains. This effect has also been reported by other researchers when organic solvents are used, the presence of enolates and alcoholates can polymerize on the nanoparticle surface producing a stabilizing effect [22,35].

3.1.4. Stability and pH

Z-Potential (ZP) provides information towards the nature of surface charge. This surface charge is responsible for attractive and repulsive forces, determining the interactions among the particles and therefore, the stability. Moreover, surface charge and particle size are factors responsible for a range of biological effects of NPs (cellular uptake, toxicity and dissolution) [36]. However it is worthwhile to mention that both magnitude and sign of zeta potential depend highly upon the concentration. The ZP values obtained are presented in Table 4.

The high values (over 20 mV) of ZP for the obtained NPs, confirm the stability of the colloidal suspensions. With the purpose of verifying the long term stability, ZP measurements were repeated after 14 days. According to the data, Cu-NPs obtained in water (samples a and c), show a remarkable stability. These results are in accordance with previous studies which show that a high oxidation state of the particle surfaces causes electrostatic repulsion, resulting in a high stability [22]. In contrast, ZP values of Cu-NPs obtained in methyl alcohol (samples b and d) decrease notably with time. This tendency to reduce the ZP values in time, approaching to the isoelectric point, shows a lower time stability and certain tendency to aggregation.

ZP and colloidal stability is also related to pH [36]. pH measurements of the obtained suspensions are reported in Table 5. According to the data, all samples present basic pH close to neutrality. After 14 days, pH values decrease. This pH decrease in time can be attributed to the absorbed carbon dioxide in solution from the ambient gas. In case of aqueous solutions, the dissociation of CO_2 in water can reduce the pH from 7 to 5.5 [37].

Although the isoelectric point (IEP) of the colloidal suspensions was not reached during our study, our results are in agreement with previous works that stablish the IEP for aqueous Cu, CuO, Cu_2O suspensions in pH values of 2.3, 4.5 and 6.5 respectively [38].

3.2. Physicochemical characterization of the immobilized nanoparticles

Due to the natural drying process, an irregular layer covers the whole surface of the titanium substrates (see Fig. 11A). FIB-prepared

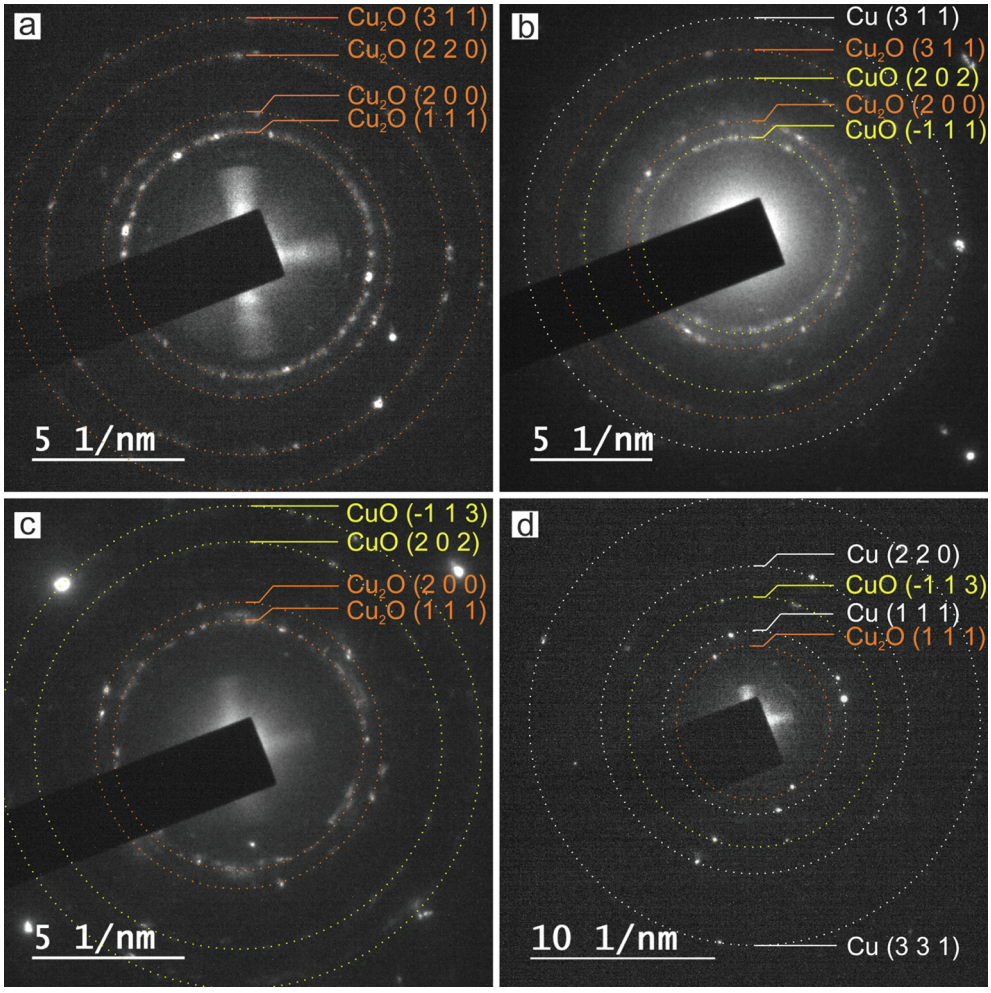

Fig. 7. SAED pattern obtained over a group of Cu nanoparticles by means of laser ablation in water using (a) pulse nanosecond laser in water, (b) pulse nanosecond laser in methyl alcohol, (c) pulse picosecond laser in water, (d) pulse picosecond laser in methyl alcohol.

Table 3
Lattice spacing measured in nm from SAED and the corresponding diffraction patterns from the ICDD database of metallic Copper, CuO and Cu_2O.

a	b	c	d	Cu (*hkl*)	CuO (*hkl*)	Cu_2O (*hkl*)
0.246		0.248	0.243			0.247 (1 1 1)
	0.252				0.252 (−1 1 1)	
			0.203	0.209 (1 1 1)		
0.214	0.216	0.212				0.214 (2 0 0)
	0.155	0.155			0.158 (2 0 2)	
		0.149	0.149		0.150 (−1 1 3)	
0.151						0.151 (2 2 0)
			0.120	0.128 (2 2 0)		
0.129	0.132					0.129 (3 1 1)
	0.110			0.109 (3 1 1)		
			0.083	0.083 (3 3 1)		

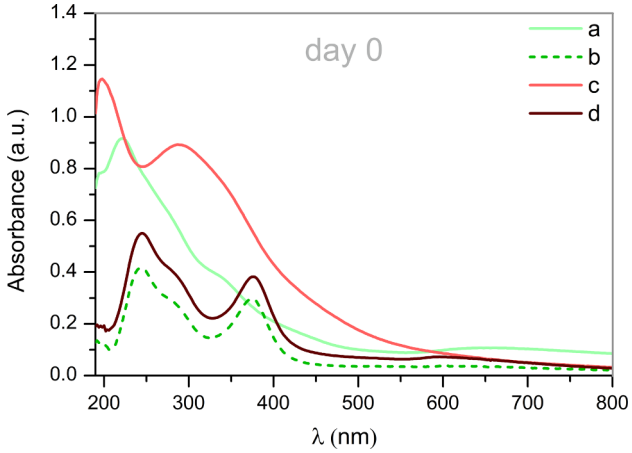

Fig. 8. UV-vis spectrum of Cu nanoparticles obtained by laser ablation using the Green – nanosecond laser in (a) water, (b) methyl alcohol and using the IR – picosecond laser in (c) water, (d) methyl alcohol.

cross-section shows the arrangement of immobilized Cu-NPs on the titanium plate (Fig. 11B and E). EDS mapping allows to identify the copper NPs layer between the Pt protecting layer and the Ti substrate (Fig. C, D).

Although the exact pathway of killing microbes by copper oxides remains unclear, few researches have addressed that ionic Cu release is behind this antimicrobial effect [30,39,40]. In order to study the ion release kinetics from the immobilized nanoparticles on Ti plates, copper ions content was measured during 21 days.

As shown in Fig. 12, samples obtained by laser ablation in water (samples a and c) show a higher rate of ion release than the others obtained in methyl alcohol (samples b and d). This difference can be attributed to the presence of the carbon protective layer on the nanoparticle surface produced when ablation takes place in methanol [35].

For all samples, the ion release seems to become stable after 7 days (168 h).

Additionally, the results obtained by measuring the absorbance of

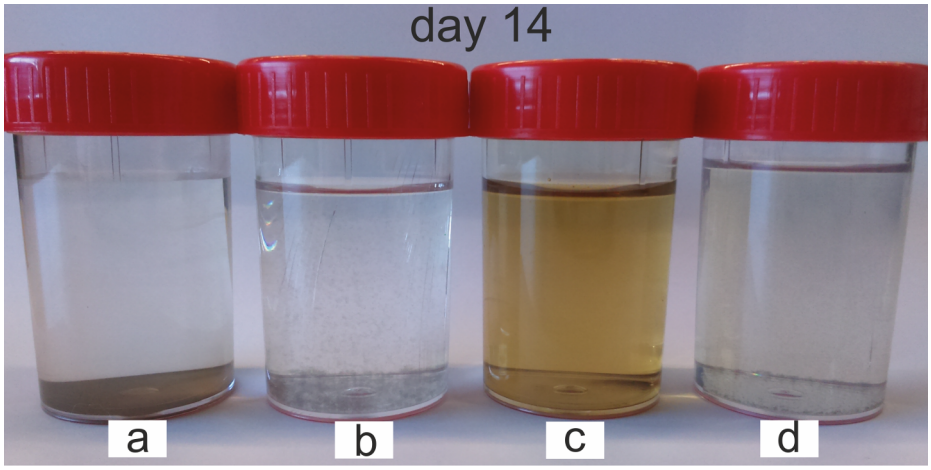

Fig. 9. (A) Photograph of the Cu-NPs suspensions 14 days after having been obtained. (B) Same samples after sonication.

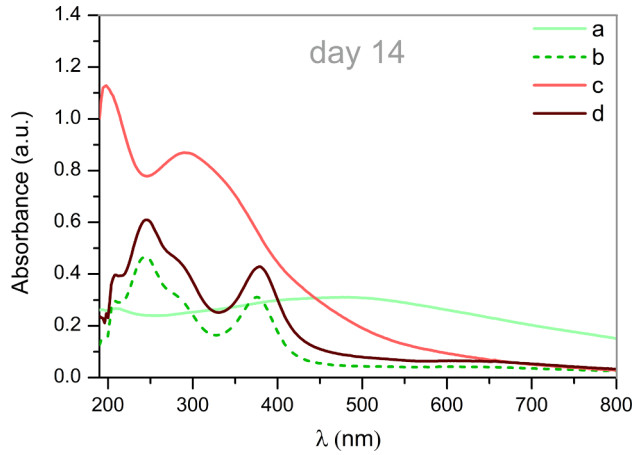

Fig. 10. UV-vis spectrum of the obtained Cu nanoparticles after 14 days.

the liquid where the Ti plates with the immobilized NPs were submerged, showed no detectable absorption peak during these 21 days, indicating that particles remain attached to the surface.

Table 4
Z-Potential measurements.

Sample	a	b	c	d
Z Potential (mV) day 0	23.8	25.1	40.6	28.2
Z Potential (mV) day 14	23.5	13.0	39.4	18.5

Table 5
pH measurements.

Sample	a	b	c	d
pH day 0	8.23	8.74	8.46	7.76
pH day 14	8.03	7.84	7.62	7.33

3.3. Bio response of the immobilized nanoparticles

3.3.1. Bacterial growth inhibition assay

The antibacterial properties of the titanium surfaces modified with the Cu-NPs was assessed against *A. actinomycetemcomitans* (Fig. 13).

The antibacterial assay reveals that *A. actinomycetemcomitans* is susceptible to the obtained Cu-NPs, showing a greater inhibitory effect for those nanoparticles obtained by laser ablation with IR – picosecond laser in water (sample c).

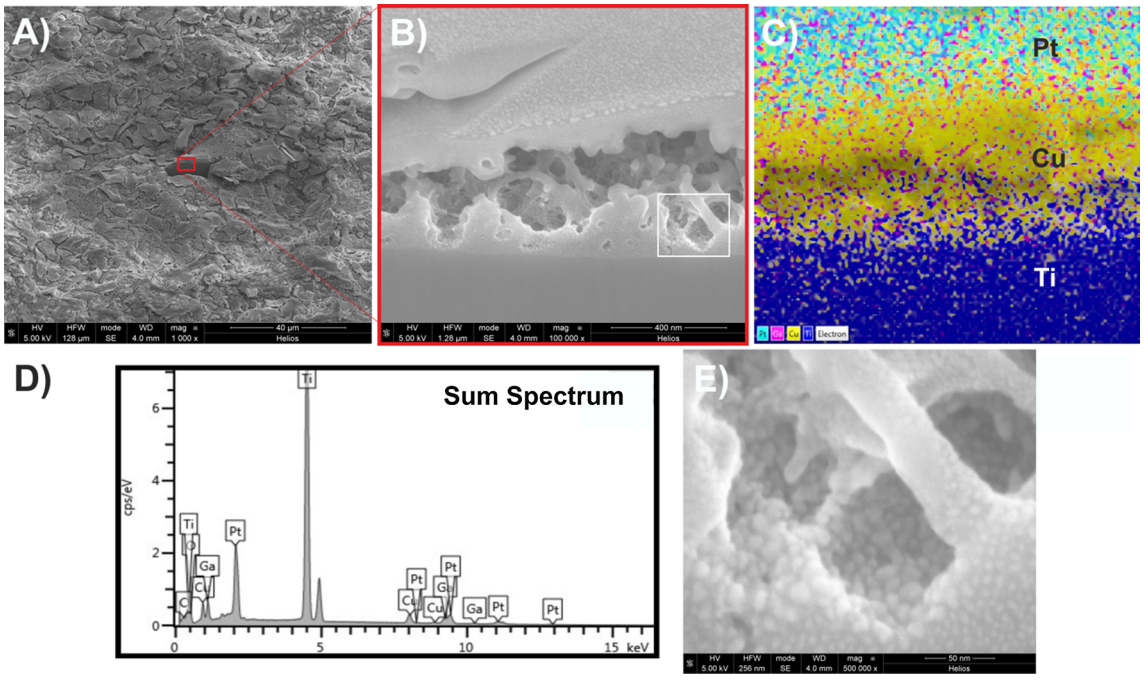

Fig. 11. (A) SEM micrograph of the thin film of Cu-NPs on the titanium plate. (B and E) SEM images of FIB-prepared cross-section showing the arrangement of immobilized Cu-NPs on the titanium plate. (C) EDS Mapping corresponding to the cross-sectional view. The elements are color-coded as clear blue for Pt, yellow for Cu, dark blue for Ti and pink for Ga ions. (D) Sum spectrum obtained from the cross-section. (For interpretation of the references to colour in this figure legend, the reader is referred to the web version of this article.)

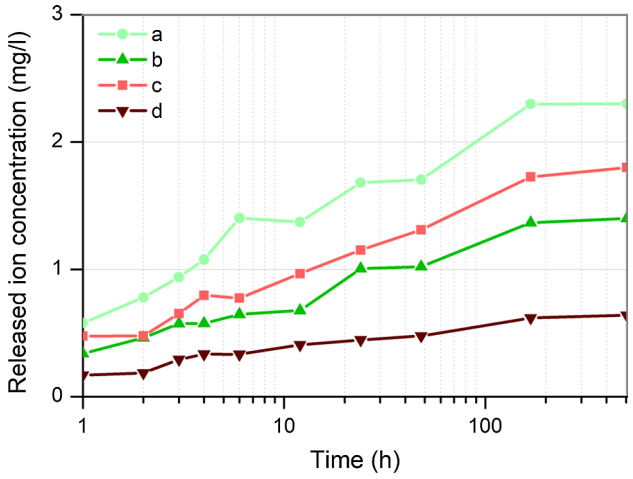

Fig. 12. Kinetics of copper ion release from the immobilized copper nanoparticles on Ti plates.

Comparing the effects of the samples with each other, we can observe that those obtained in water (samples a and c) have a greater bactericidal effect comparing with the analogous obtained in methyl alcohol (samples b and d, respectively). These results confirm that copper oxide increases substantially the antimicrobial activity [26,41].

Moreover, Cu-NPs obtained by using the IR – picosecond laser (samples c and d) are potentially more effective than those obtained with the Green – nanosecond laser (samples a and b). Even though previous studies stablish a direct relationship between smaller particle size and higher antibacterial activity of Cu-NPs [30], our results seem to suggest the influence of a preferred particle size. According to this, the presence of larger particles seems to make the bactericidal process more effective. Whereas morphology does not seem to influence the process significantly.

These results confirm that unlike silver, ions release is not the main responsible parameter for the bactericidal activity of copper nanoparticles [42].

3.3.2. Cell culture

In order to verify that colloidal suspensions are effective against bacteria, but do not produce harmful effects for healthy tissues, we have carried out cytocompatibility analysis of those suspensions. Cell proliferation and viability was performed with human periodontal ligament stem cells (PDLSCs), and a live/dead assay was conducted to evaluate the cell viability. The results of in vitro tests indicate that the samples with nanoparticles present statistically similar results to bare Ti

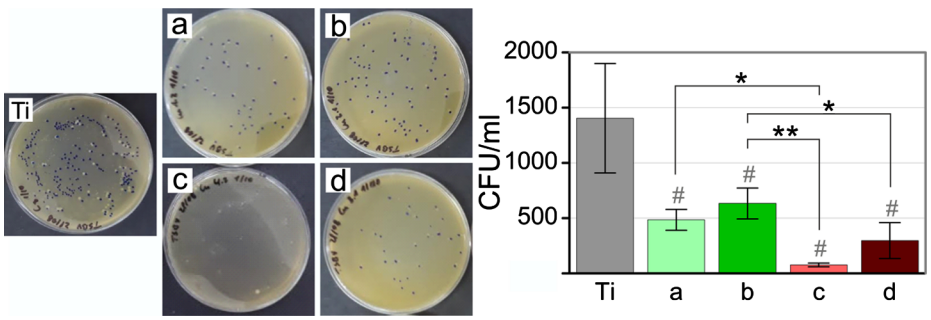

Fig. 13. Antibacterial activity of Titanium with Cu nanoparticles obtained by laser ablation using (a) pulse nanosecond laser in water, (b) pulse nanosecond laser in methyl alcohol, (c) pulse picosecond laser in water, (d) pulse picosecond laser in methyl alcohol compared with the control (Titanium discs without nanoparticles). Data is presented in form of mean ± SD. In each group, n = 3. Significant difference of each group with the control group (#p–value < 0.05) and significant difference among the different experimental groups (*p–value < 0.05 and **p-value < 0.01).

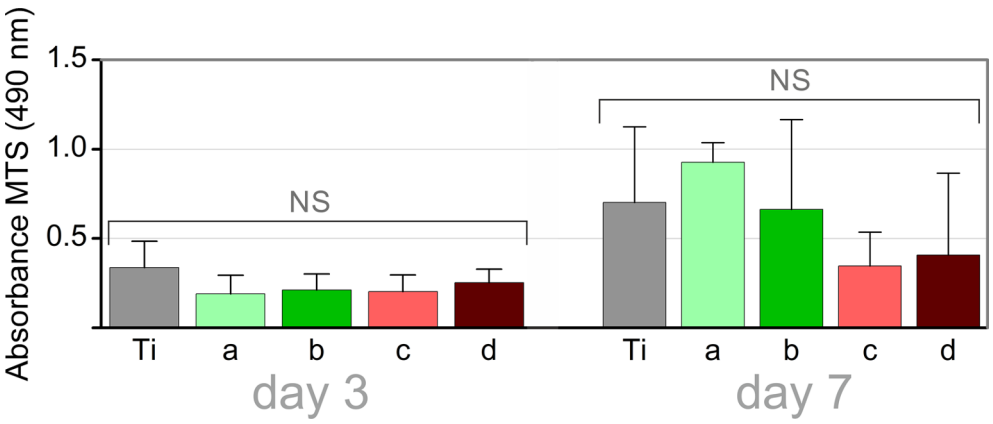

Fig. 14. MTS viability of Titanium with Cu nanoparticles obtained by laser ablation using (a) pulse nanosecond laser in water, (b) pulse nanosecond laser in methyl alcohol, (c) pulse picosecond laser in water, (d) pulse picosecond laser in methyl alcohol compared with the control (Titanium discs without nanoparticles). Data is presented in form of mean ± SD. In each group, n = 3. The difference between each group and the control group is not significant (ns, p–value > 0.05).

used as biocompatible control, as can be seen from Fig. 14.

4. Conclusions

Feasibility of laser ablation of solids in liquids to produce crystalline copper nanoparticles without any additional chemical compound is demonstrated. The type of solvent has more influence over size and stability of the obtained nanoparticles than the laser source used and determines to a large extent the characteristics of the nanoparticles.

Cu-NPs obtained by laser ablation in methyl alcohol are spherical with low degree of oxidation, while those obtained in water present chain-like nanostructure and correspond with a total oxidation state. All obtained NPs are crystalline and its high stability seems to be related to a high oxidation state. On its behalf, Cu-NPs obtained with the Green – nanosecond laser are smaller and homogeneous in size than those obtained by using the IR – picosecond laser.

The obtained results from the biological assays confirm that unlike silver, ions release is not the main responsible parameter in the bactericidal activity of copper nanoparticles. Other factors such as oxidation state, size and crystallographic structure of the nanoparticles, have a greater influence on the process.

Bactericidal activity of produced Cu nanoparticles against *Aggregatibacter actinomycetemcomitans* as well as their cytocompatibility encourages their use as anti- periimplantitis agent in oral implants.

Author Contributions

M. Fernández-Arias: Collected the data, Performed the analysis, Wrote the paper. M. Boutinguiza: Conceived and designed the analysis, Performed the analysis, Wrote the paper. J. Del Val: Contributed data or analysis tools, Other contribution: Graphic design. C. Covarrubias: Conceived and designed the analysis, Collected the data. F. Bastias: Contributed data or analysis tools. L. Gómez: Performed the analysis. M. Maureira: Collected the data. F. Arias-González: Contributed data or analysis tools, Performed the analysis. A. Riveiro: Contributed data or analysis tools. J. Pou: Conceived and designed the analysis, Performed the analysis, Wrote the paper.

Declaration of Competing Interest

The authors declare that they have no known competing financial interests or personal relationships that could have appeared to influence the work reported in this paper.

Acknowledgements

This work was partially supported by the EU research project Bluehuman (EAPA_151/2016 Interreg Atlantic Area), Government of Spain [RTI2018-095490-J-I00 (MCIU/AEI/FEDER, UE)], and by Xunta de Galicia (ED431B 2016/042, ED481D 2017/010, ED481B 2016/047-0). The technical staff from CACTI (University of Vigo) is gratefully acknowledged. C. Covarrubias acknowledges support from Project U-Redes NanoBioMat, University of Chile.

References

[1] B. Li, T.J. Webster, Bacteria antibiotic resistance: new challenges and opportunities for implant-associated orthopaedic infections, J. Orthop. Res. 36 (2018) 22–32, https://doi.org/10.1002/jor.23656.
[2] C.L. Ventola, The antibiotic resistance crisis Part 1: causes and threats, P&T 40 (2015) 277–283.
[3] A. Raghunath, E. Perumal, Metal oxide nanoparticles as antimicrobial agents: a promise for the future, Int. J. Antimicrob. Agents. (2017), https://doi.org/10.1016/j.ijantimicag.2016.11.011.
[4] D. Koulenti, A. Song, A. Ellingboe, M.H. Abdul-aziz, P. Harris, E. Gavey, J. Lipman, Infections by multidrug-resistant Gram-negative Bacteria: what's new in our arsenal and what's in the pipeline? Int. J. Antimicrob. Agents. 53 (2019) 211–224, https://doi.org/10.1016/j.ijantimicag.2018.10.011.
[5] L.J.A. Heitz-Mayfield, N.P. Lang, Comparative biology of chronic and aggressive periodontitis vs. peri-implantitis, Periodontol 53 (2010) (2000) 167–181, https://doi.org/10.1111/j.16000757.2010.00348.
[6] J. Mouhyi, D.M. Dohan Ehrenfest, T. Albrektsson, The Peri-Implantitis : Implant Surfaces, Microstructure, and Physicochemical Aspects, Clin. Implant Dent. Relat. Res. 14 (2009) 170–183, https://doi.org/10.1111/j.1708-8208.2009.00244.x.
[7] L.G. Rubin, 181 – Other Gram-Negative Coccobacilli, 5th Ed., Elsevier Inc., 2018 10.1016/B978-0-323-40181-4.00181-X.
[8] H. Khalid, S. Shamaila, N. Zafar, R. Sharif, J. Nazir, M. Rafique, Antibacterial behavior of laser-ablated copper nanoparticles, Acta Metall. Sin. (English Lett.) 29 (2016) 748–754, https://doi.org/10.1007/s40195-016-0450-x.
[9] K.M. Rajesh, B. Ajitha, Y.A. Kumar, Y. Suneetha, P.S. Reddy, Synthesis of copper nanoparticles and role of pH on particle size control, Mater. Today Proc. 3 (2016) 1985–1991, https://doi.org/10.1016/j.matpr.2016.04.100.
[10] D.O.O. Galindo, E.O. Contreras, Copper nanoparticles by laser ablation confined in methanol in the presence of an argon gas environment, J. Laser Micro Nanoeng. 12 (2017) 304–306, https://doi.org/10.2961/jlmn.2017.03.0021.
[11] J.R. Morones, J.L. Elechiguerra, A. Camacho, K. Holt, J.B. Kouri, J.T. Ramírez, M.J. Yacaman, The bactericidal effect of silver nanoparticles, Nanotechnology 16 (2005) 2346–2353, https://doi.org/10.1088/0957-4484/16/10/059.
[12] M. Boutinguiza, M. Fernández-Arias, J. del Val, J. Buxadera-Palomero, D. Rodríguez, F. Lusquiños, F.J. Gil, J. Pou, Synthesis and deposition of silver nanoparticles on cp Ti by laser ablation in open air for antibacterial effect in dental implants, Mater. Lett. 231 (2018) 126–129, https://doi.org/10.1016/j.matlet.2018.07.134.
[13] M. Fernández-Arias, M. Boutinguiza, J. del Val, E. Medina, D. Rodríguez, A. Riveiro, R. Comesaña, F. Lusquiños, F.J. Gil, J. Pou, RE-irradiation of silver nanoparticles obtained by laser ablation in water and assessment of their antibacterial effect, Appl. Surf. Sci. 473 (2019) 548–554, https://doi.org/10.1016/j.apsusc.2018.12.182.
[14] S. Grade, J. Eberhard, P. Wagener, A. Winkel, C.L. Sajti, S. Barcikowski, M. Stiesch, Therapeutic window of ligand-free silver nanoparticles in agar-embedded and colloidal state: in vitro bactericidal effects and cytotoxicity, Adv. Biomater. 14 (2012) 231–239, https://doi.org/10.1002/adem.201180016.
[15] A. Nath, A. Khare, Size induced structural modifications in copper oxide nanoparticles synthesized via laser ablation in liquids, J. Appl. Phys. 110 (2011), https://doi.org/10.1063/1.3626463.
[16] R.M. Tilaki, A.I. Zad, S.M. Mahdavi, Size, composition and optical properties of copper nanoparticles prepared by laser ablation in liquids, Appl. Phys. A 88 (2007) 415–419, https://doi.org/10.1007/s00339-007-4000-2.
[17] M. Muniz-Miranda, C. Gellini, A. Simonelli, M. Tiberi, F. Giammanco, E. Giorgetti, Characterization of copper nanoparticles obtained by laser ablation in liquids, Appl. Phys. A 110 (2013) 829–833, https://doi.org/10.1007/s00339-012-7160-7.

[18] B. Henderson, J.M. Ward, D. Ready, Aggregatibacter (Actinobacillus) actinomycetemcomitans: a triple A * periodontopathogen? Periodontol. 2000 (54) (2010) 78–105.
[19] C. Covarrubias, A. Agüero, M. Maureira, E. Morelli, G. Escobar, F. Cuadra, C. Peñafiel, A. Von Marttens, In situ preparation and osteogenic properties of bionanocomposite scaffolds based on aliphatic polyurethane and bioactive glass nanoparticles, Mater. Sci. Eng. C 96 (2019) 642–653, https://doi.org/10.1016/j.msec.2018.11.085.
[20] G.W. Yang, Laser ablation in liquids: applications in the synthesis of nanocrystals, Prog. Mater. Sci. 52 (2007) 648–698, https://doi.org/10.1016/j.pmatsci.2006.10.016.
[21] C. Pang, J. Jung, J.W. Won, Y.T. Tae, Thermal conductivity measurement of methanol-based nanofluids with Al2O3 and SiO2 nanoparticles, Int. J. Heat Mass Transf. 55 (2012) 5597–5602, https://doi.org/10.1016/j.ijheatmasstransfer.2012.05.048.
[22] G. Marzun, H. Bönnemann, C. Lehmann, B. Spliethoff, C. Weidenthaler, S. Barcikowski, Role of dissolved and molecular oxygen on Cu and PtCu alloy particle structure during laser ablation synthesis in liquids, Chemphyschem 18 (2017) 1–11, https://doi.org/10.1002/cphc.201601315.
[23] V. Amendola, M. Meneghetti, Laser ablation synthesis in solution and size manipulation of noble metal nanoparticles, Phys. Chem. C 11 (2009) 3805–3821, https://doi.org/10.1039/b900654k.
[24] M. Maina, Y. Okamoto, R. Inoue, S. Nakashiba, A. Okada, T. Sakagawa, Influence of surface state in micro-welding of copper by Nd:YAG laser, Appl. Sci. 8 (2018) 2364, https://doi.org/10.3390/app8122364.
[25] T. Tsuji, K. Iryo, N. Watanabe, M. Tsuji, Preparation of silver nanoparticles by laser ablation in solution: influence of laser wavelength on particle size.pdf, Appl. Surf. Sci. 202 (2002) 80–85.
[26] T. Jayaramudu, K. Varaprasad, R.D. Pyarasani, K.K. Reddy, K.D. Kumar, A. Akbari-Fakhrabadi, R.V. Mangalaraja, J. Amalraj, Chitosan capped copper oxide/copper nanoparticles encapsulated microbial resistant nanocomposite films, Int. J. Biol. Macromol. 128 (2019) 499–508, https://doi.org/10.1016/j.ijbiomac.2019.01.145.
[27] H. Khanehzaei, M.B. Ahmad, K. Shameli, Z. Ajdari, Synthesis and characterization of Cu @ Cu 2 O core shell nanoparticles prepared in seaweed Kappaphycus alvarezii media, Int. J. Electrochem. Sci. 9 (2014) 8189–8198.
[28] R. Raghav, P. Aggarwal, S. Srivastava, Tailoring oxides of copper-Cu2O and CuO nanoparticles and evaluation of organic dyes degradation, AIP Conf. Proc. 1724 (2016), https://doi.org/10.1063/1.4945198.
[29] J. Zhu, D. Li, H. Chen, X. Yang, L. Lu, X. Wang, Highly dispersed CuO nanoparticles prepared by a novel quick-precipitation method, Mater. Lett. 58 (2004) 3324–3327, https://doi.org/10.1016/j.matlet.2004.06.031.
[30] S. Prakash, N. Elavarasan, A. Venkatesan, K. Subashini, M. Sowndharya, V. Sujatha, Green synthesis of copper oxide nanoparticles and its effective applications in Biginelli reaction, BTB photodegradation and antibacterial activity, Adv. Powder Technol. 29 (2018) 3315–3326, https://doi.org/10.1016/j.apt.2018.09.009.
[31] J. Díaz-Visurraga, C. Daza, C. Pozo, A. Becerra, C. von Plessing, A. García, Study on antibacterial alginate-stabilized copper nanoparticles by FT-IR and 2D-IR correlation spectroscopy, Int. J. Nanomed. 7 (2012) 3597–3612, https://doi.org/10.2147/IJN.S32648.
[32] S.S. Sawant, A.D. Bhagwat, C.M. Mahajan, Novel facile technique for synthesis of stable cuprous oxide (Cu2O) nanoparticles – an ageing effect, J. Nano- Electron. Phys. 8 (2016) 1–4, https://doi.org/10.21272/jnep.8(1).01036.
[33] S.S. Sawant, A.D. Bhagwat, C.M. Mahajan, Synthesis of cuprous oxide (Cu2O) nanoparticles – a review, J. Nano- Electron. Phys. 8 (2016) 1–5, https://doi.org/10.21272/jnep.8(1).01035.
[34] K.S. Khashan, M.S. Jabir, F.A. Abdulameer, Carbon nanoparticles decorated with cupric oxide nanoparticles prepared by laser ablation in liquid as an antibacterial therapeutic agent, Mater. Res. Exp. (2018), https://doi.org/10.1088/2053-1591/aab0ed.
[35] G. Cristoforetti, E. Pitzalis, R. Spiniello, R. Ishak, F. Giammanco, M. Muniz-Miranda, S. Caporali, Physico-chemical properties of Pd nanoparticles produced by Pulsed Laser Ablation in different organic solvents, Appl. Surf. Sci. 258 (2012) 3289–3297, https://doi.org/10.1016/j.apsusc.2011.11.084.
[36] S. Bhattacharjee, DLS and zeta potential – what they are and what they are not? J. Control. Release 235 (2016) 337–351, https://doi.org/10.1016/j.jconrel.2016.06.017.
[37] N. Wang, C. Hsu, L. Zhu, S. Tseng, J. Hsu, Influence of metal oxide nanoparticles concentration on their zeta potential, J. Colloid Interface Sci. 407 (2013) 22–28, https://doi.org/10.1016/j.jcis.2013.05.058.
[38] A. Nennemann, M. Voetz, G. Hey, L. Puppe, S. Kirchmeyer, Smart colloidal materials, in: W. Richtering (Ed.), Prog. Colloid Polym. Sci. Springer-Verlag, Berlin, Heidelberg, 2006, pp. 159–168 doi: 0.1007/3-540-32702-9.
[39] C. Gunawan, W.Y. Teoh, C.P. Marquis, R. Amal, Cytotoxic origin of copper (II) oxide nanoparticles: comparative studies and metal salts, ACS Nano 7214–7225 (2011).
[40] S. Meghana, P. Kabra, S. Chakraborty, N. Padmavathy, Understanding the pathway of antibacterial activity of copper oxide nanoparticles, RSC Adv. 5 (2015) 12293–12299, https://doi.org/10.1039/C4RA12163E.
[41] H.L. Karlsson, P. Cronholm, J. Gustafsson, L. Möller, Copper oxide nanoparticles are highly toxic: a comparison between metal oxide nanoparticles and carbon nanotubes, Chem. Res. Toxicol. 21 (2008) 1726–1732, https://doi.org/10.1021/tx800064j.
[42] A.E. Nel, L. Mädler, D. Velegol, T. Xia, E.M.V. Hoek, P. Somasundaran, F. Klaessig, V. Castranova, M. Thompson, Understanding biophysicochemical interactions at the nano–bio interface, Nature 8 (2009) 543–557, https://doi.org/10.1038/nmat2442.